Int. J. Electrochem. Sci., 8 (**2013**) 6905 - 6921

International Journal of
ELECTROCHEMICAL
SCIENCE
www.electrochemsci.org

Characterization and Conduction Mechanism of $La_{5/8}Sr_{3/8}MnO_3$ Thin Films Prepared by Pulsed Laser Deposition on Different Substrates

M. Navasery[1,*], *S.A. Halim*[1,*], *G.Bahmanrokh*[1], *M .Erfani H*[1], *N.Soltani*[1], *A.Dehzangi*[2], *A. Kamalianfar*[1], *F.Ud Din*[1], *S. Abdolmohammadi*[3], *S.K.Chen*[1] , *K.P.Lim*[1] , *L.A.Mehdipour*[1] *and A.Anuar* [1]

[1] Department of Physics, Science Faculty, University Putra Malaysia, 43400 UPM Serdang, Selangor, Malaysia.
[2] Institute of Microengineering and Nanoelectronics (IMEN), University Kebangsaan Malaysia, 43600 Bangi, Selangor, Malaysia.

[3]Department of Chemistry, Faculty of Science, University Putra Malaysia, 43400 UPM Serdang, Selangor, Malaysia
[*]E-mail: navaseri@gmail.com; ahalim@science.upm.edu.my

Received: 19 September 2012 / *Accepted:* 27 March 2013 / *Published:* 1 May 2013

The $La_{5/8}Sr_{3/8}MnO_3$ (LSMO) thin films were directly grown on MgO and Si wafer substrates by Pulsed Laser Deposition (PLD) technique. The films were characterized using X-ray diffraction (XRD), field emission-scanning electron microscope (FE-SEM). The electrical and magnetic properties of films are studied. From the XRD patterns, the films are found polycrystalline single-phases. The highest magnetoresistance (MR) value obtained was −17.21% for LSMO/MgO film followed by −15.65% for LSMO/Si film at 80K in a 1T magnetic field. Transition temperature (T_P) is 224K for LSMO/MgO and 200K for LSMO/Si film. The films exhibit a ferromagnetic transition at temperature (T_C) around 363K for LSMO/MgO and 307K for LSMO/Si film. For LSMO/MgO, the high Curie temperature such as 363K is one of the high T_C in all LSMO thin films and as our knowledge, is the highest value that is reported in literature for MgO substrates with high lattice mismatch parameter. The conduction mechanisms for both films have been extensively investigated. In the metallic regime, resistivity seems to emanate from the electron–electron (major) and electron-magnon (phonon) scattering processes. For both films in the range of $T > T_P$, the resistivity data were well fitted by both variable range hopping (VRH) and small polaron hopping (SPH) models giving higher density state, and lower activation energy and Mott temperature T_0 for LSMO/Si film than those for LSMO/MgO film. The high T_C such as 363K makes these LSMO/MgO films very useful for room temperature magnetic devices.

Keywords: Crystal structure, Thin film, Polycrystalline, Pulse laser deposition.

1. INTRODUCTION

Mixed valence manganites with the perovskite structure $RE_{1-x}M_xMnO_3$ (RE=rare earth; M = divalent) have been studied for almost 50 years. The system offers a degree of chemical flexibility which permits the relation between the oxides' structure, electronic and magnetic properties to be examined in a systematic way. Research on the manganites has stimulated many interest not only for new phenomena such as colossal magnetoresistance (CMR) but also in their potential applications for various devices such as field-sensor, magnetic reading heads and memories [1-5]. Lanthanum strontium manganite of $La_{1-x}Sr_xMnO_3$ (LSMO) with perovskite structure is representative manganites which show Colossal Magnetoresistance (CMR) effect. LSMO manganite has been intensively studied because of their high Curie temperature and high degree of spin polarization of the carriers at the Fermi level. It is well known that the double exchange (DE) interaction between pairs of Mn^{3+} and Mn^{4+} ion through an oxygen atom is responsible for the ferromagnetic and metallic properties in these manganese oxides. Many methods have been used for the preparation of thin films. Pulsed Laser Deposition (PLD) [6] and sputtering [7] are most used techniques for fabrication of epitaxial and polycrystalline LSMO thin films. However, there are many publications on epitaxial LSMO films grown on single crystal oxide substrates, like $SrTiO_3$[8] and $LaAlO_3$ [9] , still the preparation of high quality LSMO thin films grown directly on low cost substrates such as MgO [10] and silicon wafer [11] are limited. Moreover, for controlling the application cost, the using of low cost substrates should be considered for synthesis of LSMO films. In this work, polycrystalline $La_{5/8}Sr_{3/8}MnO_3$ films were successfully grown directly on MgO (100) and Si (100) wafer substrates by PLD from a LSMO stoichiometric ceramic target in oxygen atmosphere. The crystal structures, surface morphology, resistivity, magneto-transport and conduction mechanism at different temperatures is discussed. Finally, the highest value of Curie temperature (T_C) as compared with literature for LSMO film deposited directly on the full misfit substrate such as MgO is reported.

2. MATERIALS AND METHODS

The $La_{5/8}Sr_{3/8}MnO_3$ films were fabricated by pulsed laser deposition technique (Nd: YAG laser, λ=500nm). The details of preparation for target and thin films is described earlier [12]. The films were grown directly on MgO (100) and Si (100) substrates under O_2 pressure of 12mtorr. Before deposition the substrates were ultrasonically cleaned in acetone and ethanol, then subsequently dried in flowing nitrogen. The thickness of films (≈400nm) was measured using Profilometer. The crystal structure of the films was characterized by X-ray diffraction (XRD, Philips) and data were refined by the Rietveld refinement technique with X′Pert HighScore Plus program. The electrical transport properties were measured by the four-point method in the range of 100-300K. A four point probe system was used to measure the change in the resistance under an external applied magnetic field up to 1 Tesla with the measured temperature ranging from 80K to 300 K using Hall measurement system (model Lake Shore 7604). The AC Susceptibility measurements were performed using a CryoBINDT model. In addition, FESEM (Nova NanoSEM 30 series) was used to investigate the surface morphology of the LSMO films.

3. RESULTS AND DISCUSSION

The X-ray diffraction (XRD) patterns of the thin films are shown in the Fig.1. The XRD data were refined by the Rietveld method using the X Pert HighScore Plus program. The selected refined data were listed in Table 1. The films showed the same structure as bulk, which is the single phase rhombohedral with a space group of $R\bar{3}C$. It is noted that the sharp diffraction peak at 54.68° for LSMO/Si comes from the Si (100) substrate. The average crystallite size and strain values have been calculated by using Williamson – Hall's method [13]. The crystallite size (D) was 24.43 nm and 33.22 nm for LSMO/MgO and LSMO/Si respectively. In addition, the lattice strain (ε), was -0.118 and -0.072 for LSMO/MgO and LSMO/Si respectively. When the thin film deposition on the substrate induces a structural strain, due to the lattice mismatch between the film and substrate, where is obtained as $\delta\ \% = [(a_{substrate} - a_{film})/a_{substrate})] \times 100$. The Positive and negative value of lattice mismatch strain indicates tensile and compressive strain, respectively. The values of misfit strain are -0.97% and -30% for LSMO/Si and LSMO/MgO films respectively. Both thin films deposited on Si wafer and MgO substrates experienced compressive strain. On one hand, the large value of lattice mismatch of MgO in case of LSMO/MgO film and on other hands, the amorphous nature of native SiO_2 layer covering Si substrate and the chemical reactivity of Si with oxide film made a polycrystalline (non-epitaxial) growth. One can see from Table 1, that lattice parameters and unit cell volume for thin film sample are compressed when compared with LSMO bulk. As shown in Table1 the Mn-O bond length is decreased for LSMO thin films as compared to the bulk sample. Hence, the Mn-O-Mn band angle is almost same.

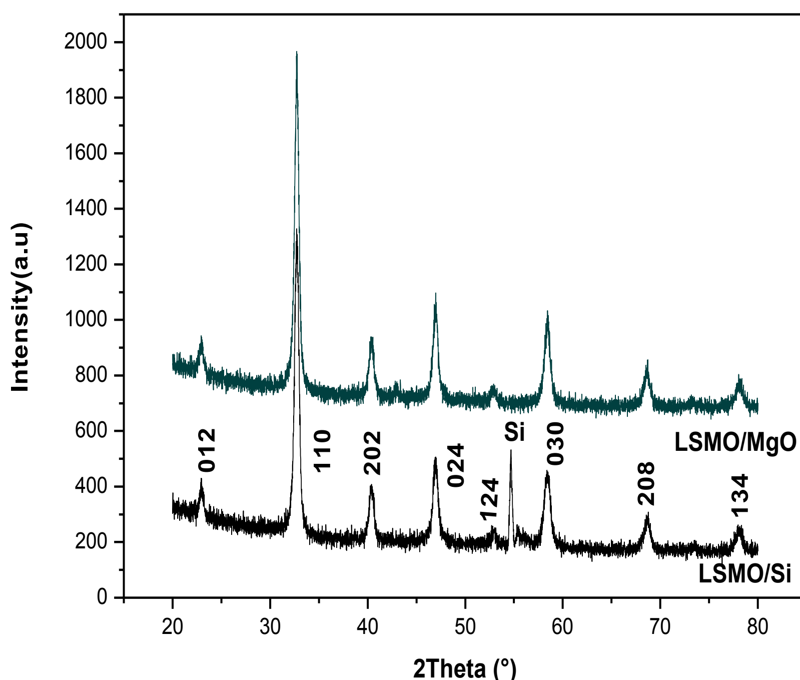

Figure 1. XRD patterns of the LSMO films are deposited on MgO (100) and Silicon (100) wafer substrates.

Table 1. Structural parameters and crystallite size of LSMO bulk and thin films.

Structural Parameters / Samples	LSMO/Si	LSMO/MgO	LSMO(Bulk)
a(Å)	5.482(7)	5.482(2)	5.489(5)
b(Å)	5.482(7)	5.482(2)	5.489(5)
c(Å)	13.340(4)	13.344(3)	13.355(2)
v(Å)^3	347.295	347.331	348.538
Lattice strain (%)	-0.118	-0.072	0.178
Cry.size(nm)	29.90	21.44	103.5
Mn-O(1)(Å)	1.945×6	1.945×6	1.948×6
Mn-O(1)-Mn(°)	167.704	167.705	167.703
R_{exp}(%)	6.5193	6.3073	5.2783
R_{pr}(%)	6.8289	5.7380	6.7636
R_{wpr}(%)	9.8754	7.1789	8.4345
Goodness of fit	2.2946	1.2954	2.5535

The surface morphologies of the films are investigated by scanning electron microscopy (SEM). Fig.2. shows the FE-SEM micrographs of LSMO films prepared at different substrates. The surface appears porous and cauliflower-like morphology for both films. The LSMO/Si thin film with smaller size of droplets and nano-cracks had smoother surface compared to the LSMO/MgO film. The average grain size of LSMO/Si and LSMO/MgO were 33.22 nm and 24.43 nm. The grain size distribution is analyzed based on 100 grains are taken from SEM micrographs of each sample. The surface morphology showing an island-like mode for deposited films. In fact, the growth of film is layer-by-layer and the lattice misfit between film and substrate lead to island growth [14].

The %MR values versus applied magnetic field H at 1 T, from 80 K to 300 K for both samples, are shown in Fig.3. The magnetoresistance ratio MR, is defined as MR = 100 × (R_H −R_0)/R_0, where R_H and R_0 reflect the resistance measured with and without a magnetic field, respectively. Both films are shown negative MR values with a vertically applied magnetic field. The results showed that the resistivity decreases with an increase in the magnetic field.

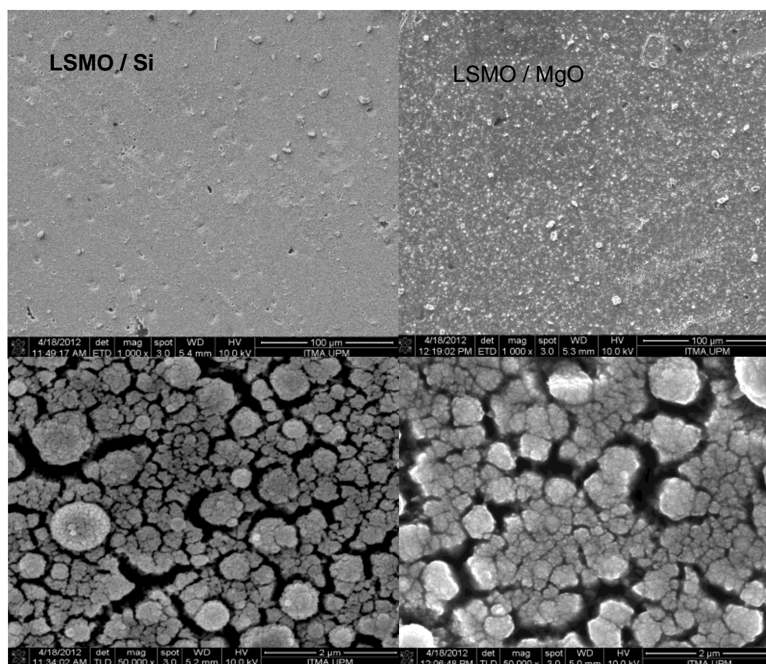

Figure 2. FE-SEM micrographs of LSMO/Si and LSMO/MgO thin films with magnification of 1KX, 50KX.

Magnetoresistance (MR) is observed in a wide temperature range below the ferromagnetic transitions. The presence of low temperature MR, may be originates from spin-dependent scattering of polarized electrons at the grain boundaries. The highest MR value obtained was −17.21% for LSMO/MgO film followed by −15.65% for LSMO/Si film at 80K in a 1 T magnetic field. The film deposited on MgO displays higher MR due to enhanced spin polarization tunnelling induced by grain boundaries effect [15] .

Fig.4. shows the temperature dependence of real part of AC susceptibility for LSMO/MgO and LSMO/Si thin film in AC field amplitude of 1 Oe and frequency of 240 Hz. Both samples show the paramagnetic to ferromagnetic transition. The Curie temperature, Tc is found from the peak in the $d\chi'/dT$ via temperature curve that is shown in Figure 4. The T_C is 363K for LSMO/MgO and 307K for LSMO/Si thin film that is given in Table 2.. The T_C of LSMO/MgO thin film as 363K is the highest value that is reported in literature for LSMO film deposited on MgO substrates [10, 16-20]. The Curie temperature of LSMO/MgO film is higher than the bulk (331K) and is one of the highest in all reported of LSMO films deposited on various single crystal substrates [11, 21-24]. The difference between T_C and T_P is calculated, $\Delta T=T_C-T_P$ and is given in Table 2.. The larger ΔT for LSMO/MgO film may be attributed to the local inhomogeneities in magnetic and electronic transport behaviors, exist disorder and inhomogeneous occupations on A-site by rare earth ions or the oxygen nonstoichiometry, smaller grain size and various grain boundaries in the sample [25].

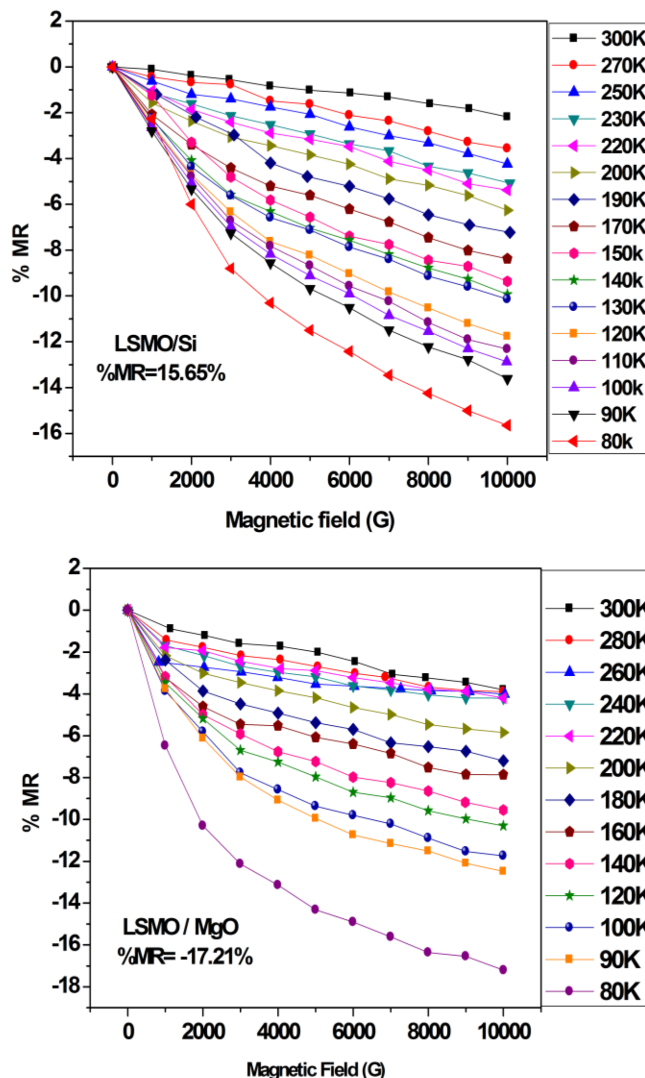

Figure 3. %MR curve of LSMO /Si and LSMO/MgO thin films as function of magnetic field at various temperatures.

Fig.5. shows normalized temperature dependent of the samples in zero magnetic field in the temperature range of 100–300 K. Phase Transition temperature (T_P) is 224 K for LSMO/MgO and 200 K for LSMO/Si film. The lower T_C and T_P for LSMO/Si may be due to interface disorders and oxygen deficiency that is caused by low oxygen- pressure during the deposition. Sahu is found that the T_C (as function of oxygen content) for LSMO/Si thin film is strongly dependent on the working pressure during sputtering [26]. The EDX results are confirmed that oxygen precenting of LSMO/Si film was lower than LSMO/MgO system. The summary of the measurement results was listed in Table 2. From Table 2 it is found that resistance of thin film deposited on MgO is much higher as compared to film deposited on Si (100) and MgO (100). The SEM studies show the grain size of LSMO/MgO film is smaller with more grain boundaries as compared to the film deposited on silicon. On other hands, the resistance of grain boundaries is more than the resistance inside the grains because of the disordered

nature of the grain boundaries. Therefore, high resistivity for LSMO/MgO is suggested to originate from the grain boundary effect.

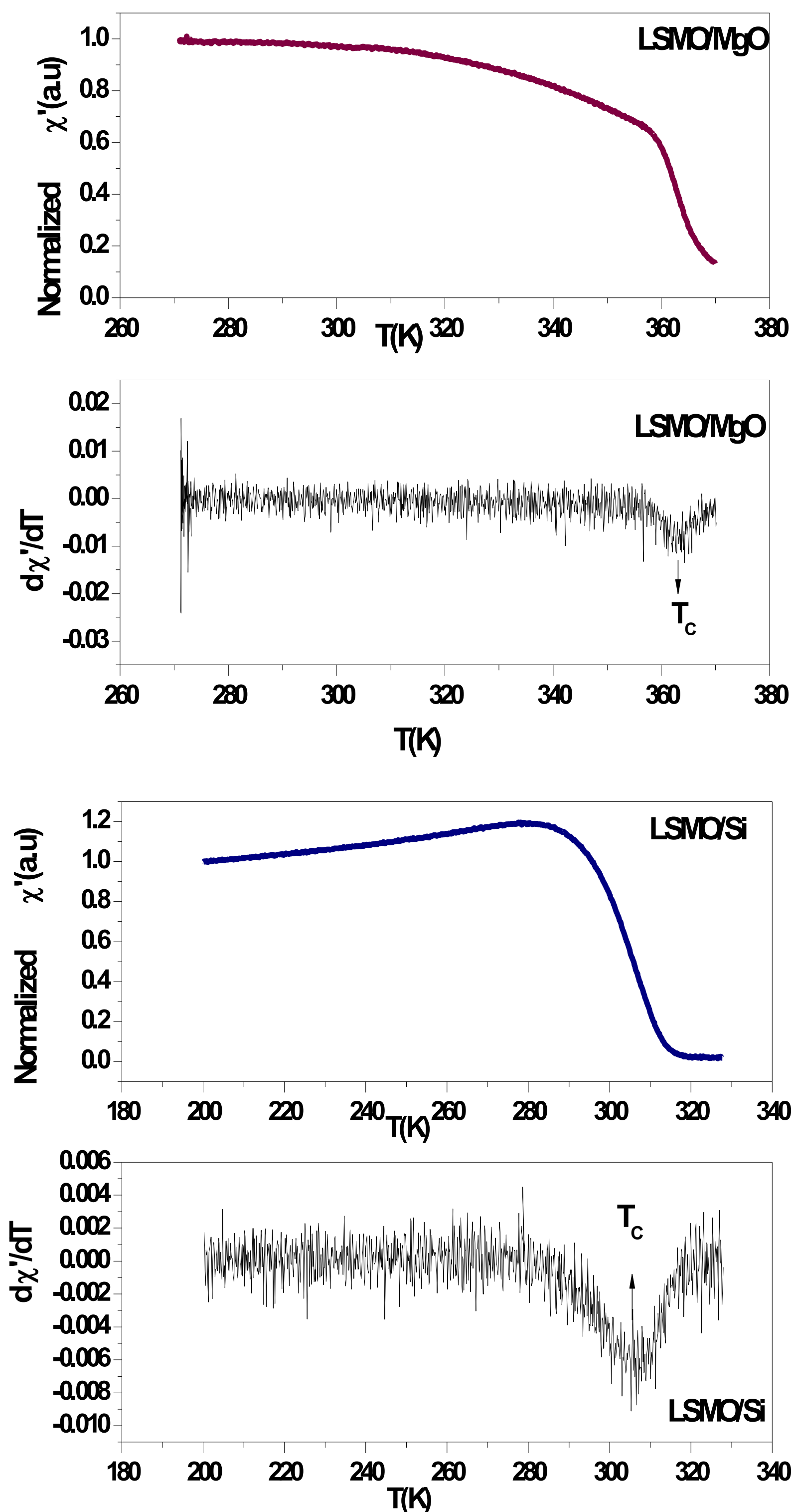

Figure 4. Temperature dependence of real part of AC susceptibility for LSMO/MgO and LSMO/Si thin films in ac field amplitude of 1 Oe.

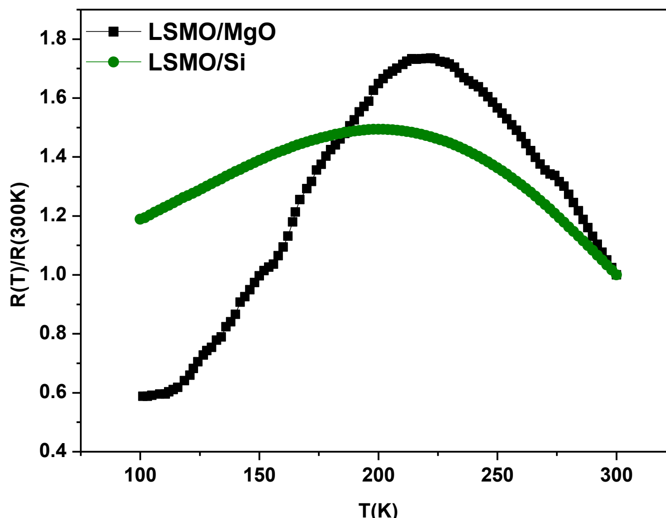

Figure 5. Temperature dependence of normalized resistance at zero magnetic field for manganite thin films.

Table 2. Summary results of LSMO films deposited on MgO (100) and Si(100) wafer.

Sample	R(100K)(KΩ)	R(300K)(KΩ)	T_P (K)	T_c (K)	ΔT(K)	S(nm)	MR%
LSMO/MgO	70.62	120.11	224	363	139	24.43	17.21
LSMO/Si	10.54	8.87	200	307	107	33.22	15.65

4. CONDUCTION MECHANISM AT DIFFERENT TEMPERATURE

4.1. Low Temperature ($T<T_P$)

In order to understand the conduction mechanism at low temperature, the electrical resistivity data are fitted using the following equations [27-30]:

$$\rho = \rho_0 + \rho_2 T^2 \qquad (1)$$

$$\rho = \rho_0 + \rho_{2.5} T^{2.5} \qquad (2)$$

$$\rho = \rho_0 + \rho_2 T^2 + \rho_{4.5} T^{4.5} \qquad (3)$$

Where ρ_0 is the temperature independent part that is due to the domain, grain boundary and other temperature independent mechanisms. The $\rho_2 T^2$ term corresponds to electron-electron scattering process and $\rho_{2.5} T^{2.5}$ term arises due to electron-magnon scattering process and $\rho_{4.5} T^{4.5}$ indicates the

resistivity due to electron–magnon scattering process in the ferromagnetic region, which may be likely to arise due to spin wave scattering process.

The experimental data for both thin films were fitted to the above equations. From the fitting results is found that the square of linear correlation coefficient R^2 for both films is the highest when the data are fitted by Eq.(3). Therefore, the conduction mechanism for both films at metallic regime seems to emanate from the electron–electron and electron-magnon (phonon) scattering processes. In addition, the electron–electron scattering term ρ_2, in Eq. (3) is larger than that of the electron–magnon (phonon) $\rho_{4.5}$ for both films. Therefore, the electron–electron scattering displays a major role on conductivity of samples in metallic regime. Fig.6.is shown the ln ρ versus temperature for samples below T_P, that is fitted with Eq.(3). The best fitted parameters are given in Table 3.. It is found that values of $\rho_{0,}$ ρ_2 and $\rho_{4.5}$ are smaller for LSMO/Si as compared to the film is deposited on MgO. The LSMO/Si film has bigger size of grain and less grain boundary region, results to decreasing of scattering parameters as well as electon-electron and electron-magnon. Therefore, the grain boundary has an effective role to enhancement of scattering of conduction electron.

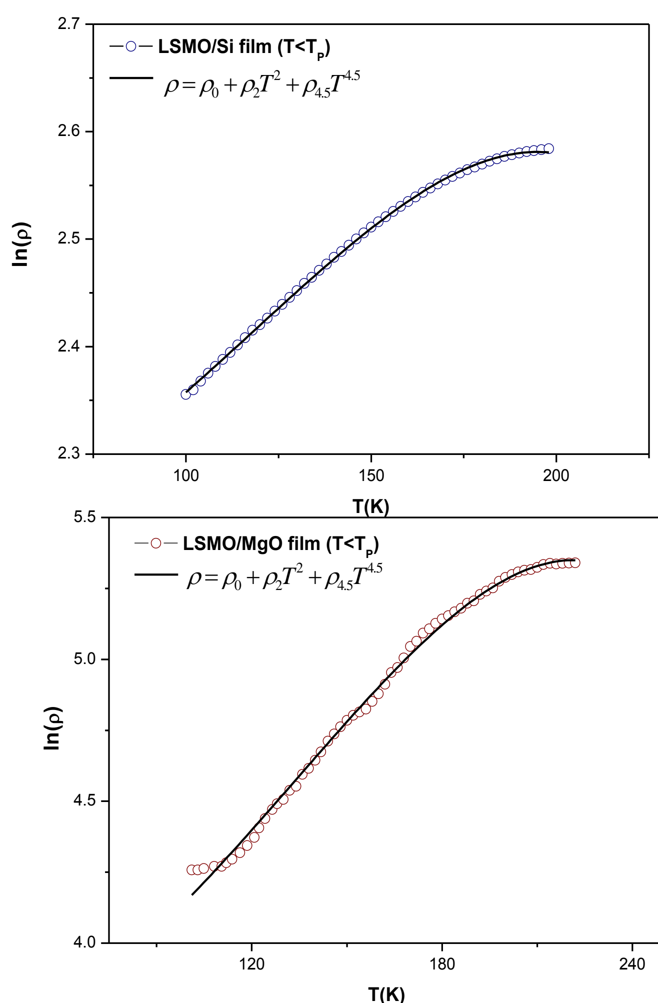

Figure 6. ln ρ versus temperature for LSMO films below T_P. The solid line representing the best fit to Eq(3).

Table 3. Parameter obtained from fitting experimental data with Eq.(3)

Sample	$\rho = \rho_0 + \rho_2 T^2 + \rho_{4.5} T^{4.5}$			
	ρ_0 (KΩ.cm)	**ρ_2 (KΩ.cm.K^{-2})**	**$\rho_{4.5}$ (KΩ.cm.K$^{-4.5}$)**	**R^2**
LSMO/MgO	3.5281	6.6859	4.67×10^{-11}	0.99634
LSMO/Si	2.1854	1.8736	1.57×10^{-11}	0.99966

4.2. High Temperature ($T > T_P$)

Two models are generally used to describing the high temperature dependence ($T > T_P$) of resistivity on the paramagnetism insulator region. These models are variable-range hopping (VRH) and small polaron hopping (SPH) ($T > \theta_{D/}2$) [31] .

4.2.1. Small Polaron Hopping (SPH)

The conduction mechanism of manganites at high temperatures ($T > \theta_{D/}2$) is mainly due to the thermally activated small polarons, that described by small polaron hopping mode could be due to either adiabatic or non-adiabatic approximations [31-32]. The temperature dependence of resistivity at $T > \theta_{D/}2$, for adiabatic and non-adiabatic approximations is expressed as:

$$\rho = \rho_0 T \exp(Ea/k_B T) \quad \text{(adiabatic)} \quad (4)$$

$$\rho = \rho_0 T^{3/2} \exp(Ea/k_B T) \quad \text{(Non-adiabatic)} \quad (5)$$

Where ρ_0 is a pre-factor; k_B is the Boltzmann constant; T is the absolute temperature, and E_a is the activation energy. The resistivity data above T_P is fitted to Eq. (4) by plotting ln (ρ/T) vs. 1/T (Fig.7.) and from the best fits, the half Debye temperature, θ_D /2, as temperature at which the slope changes from linearity can be determined. Therefore, θ_D values are 532K for LSMO/Si and 544K for LSMO/Si films are given in Table 4. By using Eq.(4) and (5), the Ln(ρ /T) and Ln(ρ /$T^{3/2}$) versus(1/T) plot was drawn separately for LSMO/Si and LSMO/MgO, and the curves are shown in Fig.8. and Fig.9. As can see in Table 5., LSMO/Si thin film has lower value of the activation energy on both adiabatic and non-adiabatic regime. The reduction of the activation energy and the residual resistivity for LSMO/Si is probably due to the larger grain size, better quality of crystal structure, and phase purity of sample. Venkataiah et al. have reported the decreasing of activation energy by the increasing of grain size in LCMO single layer manganite at different sintering temperatures. They are mention that this behavior due to enhancement of hoping of the conduction electron between neighboring sites due to the increase in interconnection between the grains as the grain size increases [33].

As one can see in Table 4, the linear correlation coefficient, R^2, values for both models are close to each other, and it is difficult to classify the systems into the adiabatic or non-adiabatic regime. Therefore, for finding the type of hopping, another mechanism is needed.

By using Holstein's relation [34], one can identify whether the hopping mechanism is in the adiabatic or non- adiabatic region. This also indicates the sizes of the polarons. According to this relation, the polaron band width J should obey the following conditions:

$J>\phi$ for adiabatic hopping and $J<\phi$ for non-adiabatic hopping conduction:

$$\phi = (\frac{2k_B T E_a}{\pi})^{1/4} (\frac{h\nu_{ph}}{\pi})^2 \qquad (6)$$

$$J \approx 0.67 h\nu_{ph} (\frac{T}{\theta_D})^{1/4} \qquad (7)$$

where the longitudinal optical phonon frequency ν_{ph} , is obtained from the relation; $h\nu_{ph} = k_B \theta_D$.

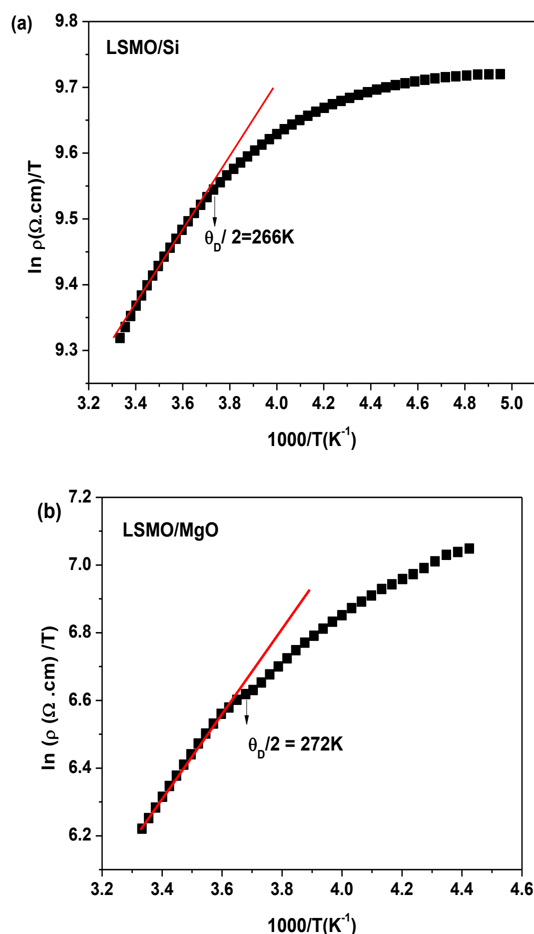

Figure 7. Inverse temperature dependence of ln(ρ/T) above T_p for (a) LSMO/Si and (b)LSMO/MgO thin films by using of SPH model.

The J value is polaron band width and T=300 K. Furthermore, the condition for small-polaron formation is J< $E_a/3$ [34]. All parameters were obtained by using Eq(6-7) are given in Table 5. It is observed that for both thin films, J< ϕ and J< $E_a/3$ on the non-adiabatic region. Therefore, we may conclude that the non-adiabatic small polaron hopping model is responsible for conduction in both thin films. It is interesting to estimate few important relevant physical parameters for both samples. The values for small-polaron coupling (γ_P), which is a measure of electron–phonon interaction in these manganites, can be evaluated from the relation $\gamma_P = E_a / h\nu_{ph}$. The value of γ_P is 3.72 for LSMO/Si and 5.05 for LSMO/MgO as shown in Table 5. It has been suggested that a value of $\gamma_P > 4$ usually indicates strong electron–phonon interaction in solids [35]. Therefore, strong and weaker electron–phonon interaction is observed for LSMO/MgO and LSMO/Si films respectively. Also from the values of γ_P, we have evaluated the ratio of the polaron mass m_P to the rigid-lattice effective mass m* using the relation $m_P = m^* \exp(\gamma_P)$ [35]. The values of mp/m* are 41.26 and 156.02 for SMO/MgO and LSMO/Si films respectively, indicating strong electron–phonon interaction for film deposited on MgO.

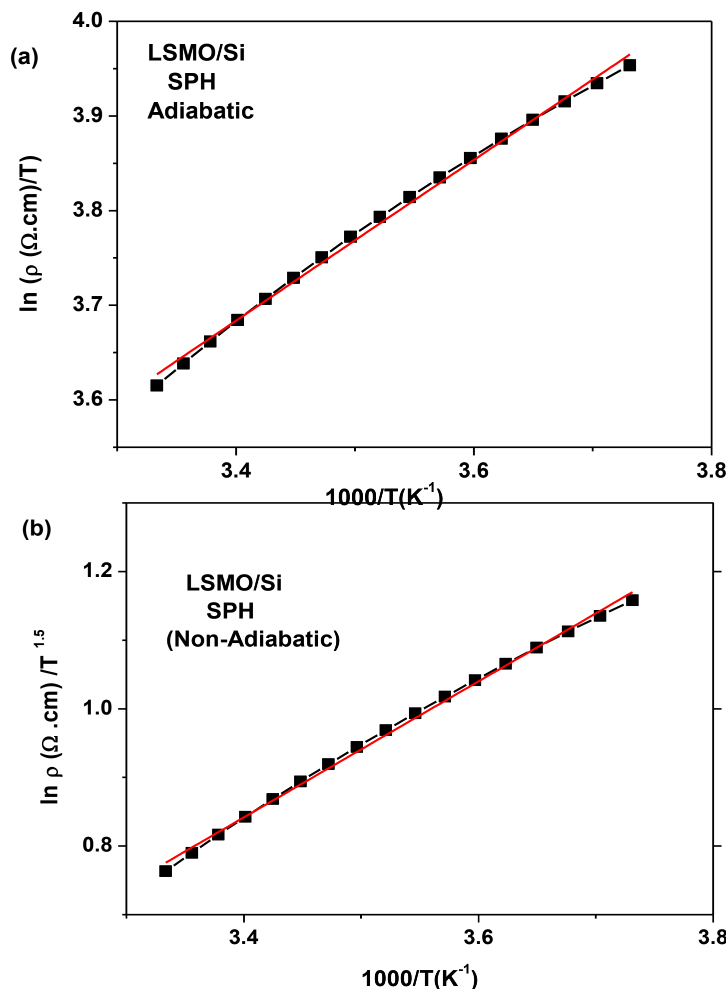

Figure 8. Ln(ρ /T) and Ln (ρ /$T^{1.5}$) versus (1/T) plot for LSMO/Si thin films above θ_D /2 (266 K) (a) for SPH –Adiabatic model (b) for SPH(Non-Adiabatic) model.

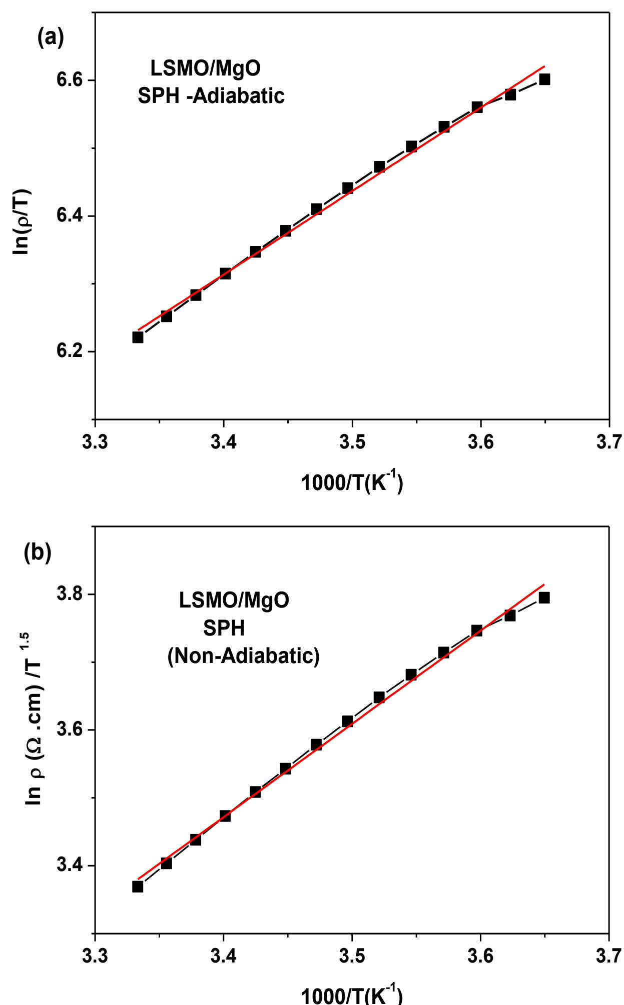

Figure 9. Ln(ρ /T) and Ln (ρ /$T^{1.5}$) versus (1/T) plot for LSMO/MgO thin films above θ_D /2 (272 K) (a) for SPH –Adiabatic model (b) for SPH(Non-Adiabatic) model.

4.2.2 Variable Range Hopping (VRH) ($T_P<T<\theta_D/2$)

The variation of the electrical resistivity with temperature above T_P and $\theta_D/2$ may be explained on the basis of variable range hopping model (VRH) model. The Mott's equation for VRH mechanism for 3D and 2D-dimention are given as [36] :

$$\rho = \rho_0 \exp (T_0/T)^{1/4} \qquad \text{3D-dimention} \qquad (8)$$

$$\rho = \rho_0 \exp (T_0/T)^{1/3} \qquad \text{2D-dimention} \qquad (9)$$

where,

$$T_0 = 16\alpha 3/k_B N (E_F) \qquad (10)$$

The constant α was taken as $2.22nm^{-1}$ [36] and N (E_F) is the density of states near the Fermi level. In order to investigate the hopping mechanism at the intermediate temperature range $T_P<T<\theta_D/2$, the resistivity data for both samples were fitted by using Eq. (8) and (9). For both thin films, the best fitting in the range of VRH is found for 3D-dimension that is shown in Fig.10. In addition, T_0 values for each film were calculated from slopes of ln(ρ) vs.$T^{-1/4}$ plot. As shown in Table 6., the calculated value of T_0 for LSMO/MgO film is higher than film deposited on Si, where N(E_F) values is lower may be due to decreasing of the double exchange (DE) interaction.

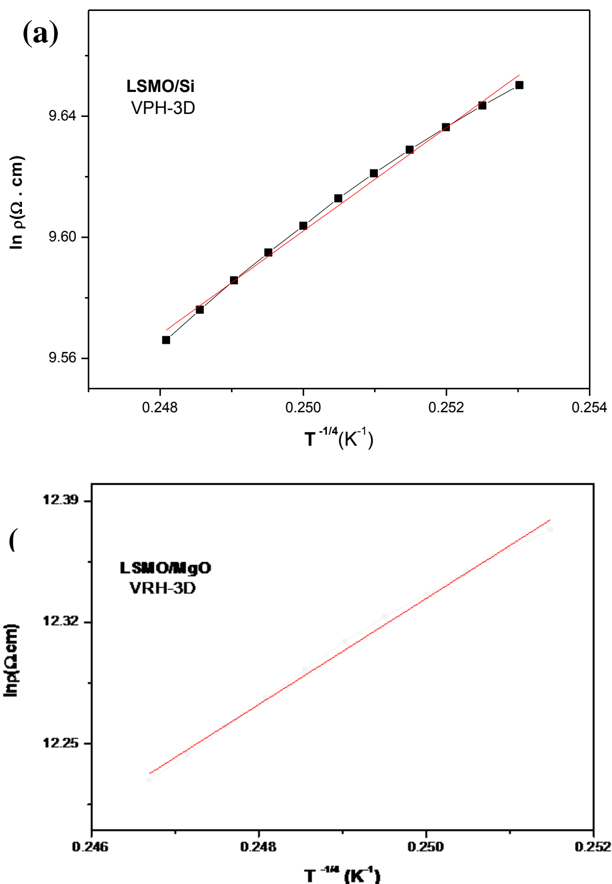

Figure 10. Ln (ρ) versus $T^{-1/4}$ for (a) LSMO/Si and (b)LSMO/MgO thin films at best fitting temperature range of VRH model. Lines represent the results for fitting 3D-VRH models.

Table 4. Parameters extracted from adiabatic and non-adiabatic SPH models.

		Adiabatic SPH		Non- Adiabatic SPH	
Samples	θ_D (K)	Ea (mev)	R^2	Ea (mev)	R^2
LSMO/Si	532	73.18	0.99619	85.40	0.99696
LSMO/MgO	544	106.05	0.99455	118.40	0.99544

Table 5. Parameters evaluated using Eq(6&7)

	Adiabatic SPH			Non- Adiabatic SPH				
Samples	Ea/3 (mev)	J (mev)	ϕ (mev)	Ea/3 (mev)	J (mev)	ϕ (mev)	γ_P	m_p/m^*
LSMO/Si	24.39	26.60	25.64	28.46	26.6	29.57	3.72	41.26
LSMO/MgO	35.35	17.32	25.59	39.46	17.32	26.30	5.05	156.02

Table 6. T_0, $N(E_F)$ and R^2 values extracted from 3-D VRH model fittings.

Sample	T_0(K)	$N(E_F)$($ev^{-1}cm^{-3}$)	R^2
LSMO/Si	8.51×10^4	2.38×10^{22}	0.99386
LSMO/MgO	8.7×10^5	2.32×10^{21}	0.99414

5. CONCLUSION

In summary, polycrystalline $La_{5/8}Sr_{3/8}MnO_3$ films were successfully deposited on MgO and Si substrates without any additional buffer layer by pulsed laser deposition. The structural characteristics, magneto-transport properties and conduction mechanism of LSMO thin films have been extensively studied. The XRD analysis showed that films are single phase rhombohedral. Both film showed island growth and cauliflower -like morphology with average grain size of 33.22 nm and 24.43 nm for LSMO/Si and LSMO/MgO respectively. The highest MR value obtained was −17.21% for LSMO/MgO film followed by −15.65% for LSMO/Si film at 80 K in a 1 T magnetic field. Transition temperature (T_P*)* is 224K for LSMO/MgO and 200 K for LSMO/Si film.

The films exhibit a ferromagnetic transition at temperature (T_C) around 363K for LSMO/MgO and 307K for LSMO/Si film. For LSMO/MgO the high Curie temperature such as 363K is one of the high T_C in all LSMO thin films and as our knowledge, is the highest value that is reported in literature for MgO substrates with high lattice mismatch parameter. The conduction mechanism for both films at metallic regime, seems to emanate from the electron–electron (major) and electron-magnon (phonon) scattering processes. For both films in the range of $T > T_P$, the resistivity data were well fitted by both variable range hopping (VRH) and small polaron hopping (SPH) models giving higher density state, and lower activation energy and Mott temperature T_0 for LSMO/Si film than those for LSMO/MgO film. The high T_C such as 363K makes these LSMO/MgO films very useful for room temperature magnetic devices.

ACKNOWLEDGMENTS
The Ministry of Science, Technology and Innovation of Malaysia is gratefully acknowledged for the grant under Science Fund vote: 9199835.

References

1. Y. Xu, U. Memmert and U. Hartmann, *Sensors and Actuators A: Physical*, 91 (2001) 26-29.
2. M. Navasery, S.A. Halim, K. P. Lim, S.K. Chen and a.R. ABD-Shukor, *Modern Physics Letter*s B, 26 (2012) 1150039-1150048.
3. M.B. Salamon and M. Jaime, *Reviews of Modern Physics*, 73 (2001) 583.
4. S.S. Balevičius, V. ; Keršulis, S. ; Schneider, M. ; Liebfried, O. ; Plaušinaitienė, V. ; Abrutis, A., *IEEE Trans. Plasma Sci*.,, 39 (2011) 411-416.
5. D. Liu and W. Liu, *Ceramics International*, 38 (2012) 2579-2581.
6. M. Gu, F. Yang, E. Arenholz, N.D. Browning and Y. Takamura, *J. Magnetism and Magnetic Materials*, 325 (2013) 69-74.
7. D. Sahu, *J. Phys. Chem. Solids*, 73 (2012) 622-625.
8. S. Seo, H. Kang, H. Jang and D. Noh, *Physical Review* B, 71 (2005) 012412-012415.
9. T. Tsuchiya, K. Daoudi, T. Manabe, I. Yamaguchi and T. Kumagai, *Appl. Surf. Sci.*, 253 (2007) 6504-6507.
10. I. Gomes, B. Almeida, A. Lopes, J. Araújo, J. Barbosa and J. Mendes, *J. Magnetism and Magnetic Materials*, 322 (2010) 1174-1177.
11. D.R. Sahua, *J. Alloys and Compounds*, 503 (2010) 163-169.
12. M.Navasery, S.A.Halim, N.Soltani, G.Bahmanrokh, K.Y.Pan, A.Kamalianfar and S.K.Chen, *Int. J. Electrochem. Sci.*, 7 (2012) article in press.
13. G. Williamson and W. Hall, *Acta Metallurgica*, 1 (1953) 22-31.
14. L. Martin, Y.H. Chu and R. Ramesh, *Mater. Sci. Engin.*: R: Reports, 68 (2010) 89-133.
15. S.Y. Pai Li, Li Liu, Xueli Wang, Yongqiang Wang, Zhaoming Tian, Jinghua He, and K.L. Shijun Yuan, Shiyan Ying, Chuanhui Wang, *Solid State Commun.*, 146 (2008) 515-521.
16. X. Zhu, H. Shen, K. Tsukamoto, T. Yanagisawa, M. Okutomi and N. Higuchi, *Ceramics International*, 38 (2012) 6405-6410.
17. P.M. Leufke and A.B. Ajay Kumar Mishra , Di Wang , Christian Kübel ,Robert Kruk , Horst Hahn, *Thin Solid Films*, 520 (2012) 5521-5527.
18. M. Spankova, S. Chromik, I. Vavra, K. Sedlackova, P. Lobotka, S. Lucas and S. Stancek, *Appl. Surf. Sci.* 253 (2007) 7599-7603.
19. M. Sirenaa and M.G. N. Haberkorna, L.B. Steren, J. Guimpel, *J. Magnetism and Magnetic Materials*, 272-276 (2004) 1171-1173.
20. S. Majumdar and H.S.M. H. Huhtinen, P. Paturi, *J. Alloys and Compounds*, 512 (2012) 332-339.
21. S.C. M. S ˇ pankova´ , I. Va´vra , K. Sedla´cˇkova´ , P. Lobotka , S. Lucas , S. Stancˇek Applied Surface Science, 253 (2007) 7599-7603.
22. B.G.A. I.T.Gomes , A.M.L.Lopes , J.P.Arau´ jo , J.Barbosa , J.A.Mendes, *J. Magnetism and Magnetic Materials*, 322 (2010) 1174-1177
23. Z.P. Shaojie Fang, Fenggong Wang, Liang Lin and Shenghao Han, *J. Mater. Sci. Technol*, 27 (2011) 223-226.
24. W.L.K. S.Y. Yang, Y. Liou, W.S. Tse, S.F. Lee, Y.D. Yao, *J. Magnetism and Magnetic Materials*, 268 (2004) 326-331.
25. J.H. Hongwei Qin, Juan Chen, Luming Zhu and Hongdong Niu, *Mater. Transactions*, 45 (2004) 1251-1254.
26. D.R. Sahu, *J. Phys. Chem. Solids*, 73 (2012) 622-625.
27. G.J. Snyder, R. Hiskes, S. DiCarolis, M.R. Beasley and T.H. Geballe, *Phys. Rev.* B, 53 (1996) 14434.
28. A. Banerjee, S. Pal and B. Chaudhuri, *J. Chem. Phys.*, 115 (2001) 1550-1558.
29. L. Pi, L. Zheng and Y. Zhang, *Phys. Rev.* B, 61 (2000) 8917-8921.
30. M.H. Ehsani, P.K. and M.E.Ghazi, *J. Phys. Chem. Solids*, 73 (2012) 744-750.
31. D. Emin and T. Holstein, *Phys. Rev. Lett.*, 36 (1976) 323.

32. N.F. Mott and E.A. Davis, Electronic processes in non-crystalline materials, Oxford Univ Pr, (2012).
33. G. Venkataiah, D. Krishna, M. Vithal, S. Rao, S. Bhat, V. Prasad, S. Subramanyam and P.V. Reddy, *Physica B: Condensed Matter*, 357 (2005) 370-379.
34. T. Holstein, *Annals of Physics*, 8 (1959) 343-389.
35. I.G.A.a.N.F. Mott, *Advanced in Physics*, 18 (1969) 41-102.
36. L.R. M. Viret, and J. M. D. Coey, *Physical Review* B, 55 (1997) 8067-8070

© 2013 by ESG (www.electrochemsci.org)